MODELING SCHEMES, TRANSIENCY, AND STRAIN MEASUREMENT FOR MICROSCALE LASER SHOCK PEENING

Hongqiang Chen, Y. Lawrence Yao
Department of Mechanical Engineering
Columbia University, New York, NY 10027

ABSTRACT

In this paper, a coupled modeling scheme, that considered the dynamic evolution of laser-induced plasma and the complete physical interaction between plasma, confined medium, coating layer and the peened metal in laser shock peeing (LSP), is compared with two decoupled modeling schemes, in which shock pressure was first determined and used as loading in subsequent FEM based stress/strain analysis. The relative merits and limitations of these schemes are evaluated in terms of their ability to describe process transiency such as shock pressure, shock velocity and dynamic deformation history, and to predict the stress/strain to be imparted into a target material. Both bulk and thin film samples of copper were studied. Model predictions were investigated together with strain measurements based on X-ray micro-diffraction technique.

INTRODUCTION

Earlier modeling work on LSP was carried out (Clauer and Holbrook, 1981). More recently, laser shock processing of copper using a micron sized beam has been studied (Zhang and Yao, 2000; 2001, 2002a & b). Modifications in model ing of LSP was made from the model (Fabbro, et al., 1990) to account for the micro scale involved (Zhang and Yao, 2000). A further improvement of the pressure model taking into account of mass, energy and momentum conservation was carried out with the plasma modeled as laser supported combustion wave and its spatial expansion effects accounted for (Zhang and Yao, 2001). Dynamic deformation process of the target material had been simulated using the finite element method (FEM) for the axisymmetric case (Zhang and Yao, 2000, 2002a). The stress and strain analysis was extended to 3D and finite geometry was considered, which again is important for micro-scale LSP (Zhang and Yao, 2001). High-spatial resolution characterization of the stress/strain fields in thin films was presented in (Zhang and Yao, 2002b).

However, there exist limitations in the work on micro-scale LSP. It was assumed that the plasma generated in LSP obeys ideal gas laws and the laser irradiation absorption is a constant. It was also assumed that density, internal energy and pressure of the plasma are uniform within the plasma volume and vary with time only. In order to simplify the calculation, the coating layer was considered to be thin and well coupled with the metal target, thus the shock pressure and the particle velocities of the coating layer

and the metal target are identical. The modeling is decoupled, in which, the shock pressure was computed firstly from the pressure model and then used as loading for the strain/stress analysis via the FEM code, assuming that the mechanical deformation will not affect the pressure evolution. In fact the process is coupled. The objective of this paper is to investigate ways to overcome these limitations.

COUPLED MODELING OF LASER SHOCK PROCESSING

To overcome the limitations of the previous modeling work, the dynamic evolution of plasma and the complete physical interaction between plasma, confined medium, coating layer (ablator) and the processed metal (target) are need to be considered as a whole.

Physical Phenomena In LSP

The mechanism of forming a high-temperature, high-pressure plasma is as follows. When laser absorption in the ablator occurs, the heated material vaporizes and the vapor rapidly achieves temperatures greater than several tens of thousands of degrees. At first, electron-neutral inverse Bremsstrahlung or multi photon ionization contributes to the creation of initial electrons, when sufficient electrons are generated, the dominant laser absorption mechanism makes a transition from electron-neutral inverse Bremsstrahlung to electron-ion inverse Bremsstrahlung. So the laser absorption of vapor becomes much stronger and the vapor is rapidly transformed into the plasma. This plasma induces shock waves during expansion from the irradiated surface, and mechanical impulses are transferred to the target.

Governing Relations In LSP

Electron Growth In LSP. The growth of electron density n_e is governed by the following equation (Weyl, 1989):

$$\frac{dn_e}{dt} = \nu_i n_e + W_m I^m n_e - \nu_a n_e - \nu_R n_e \qquad (1)$$

where W_m is the multi-photon ionization rate coefficient and I is the laser intensity, m is the number of photons that have to be absorbed simultaneously in order to ionize the gas. ν_i, ν_a and ν_R are the impact ionization, attachment, and recombination rates, respectively.

Laser absorption in LSP. The effective absorption coefficient for electron-neutral inverse Bremsstrahlung is given by (Root, 1989):

$$k'_{e,n} = \left[1 - \exp(-\frac{hc}{\lambda kT})\right] \sum_j Q_j n_e n_j \qquad (2)$$

where n_e and n_j are the number density of electron and the j^{th} neutral atomic species, Q_j is the average cross section for absorption of a photo of wavelength λ by an electron during a collision with species j, k is Boltzmann's constant, h is Planck's constant, c is velocity of light, and T is temperature. For electron-ion inverse Bresstrahlung dominates.

$$k'_{e,i} = \left[1 - \exp(-\frac{hc}{\lambda cT})\right] \frac{4e^6\lambda^3}{3hc^4 m_e} (\frac{2\pi}{3m_e kT})^{\frac{1}{2}} n_e \sum_j z_i^2 n_i g_i \qquad (3)$$

where z_i and n_i are the charge and number density of the i^{th} ionic species, and g_i is the appropriate Gaunt factor that corrects the semi-classical expression for quantum effects, m_e is the mass of the electron.

Ionization model. Because the laser pulse width in LSP is 50 ns, which is much larger then the electron-ion collision time, τ_{ei}, the ion formation can be treated within the framework of the local thermal equilibrium theory (LTE) and it is possible to employ the Boltzmann and Saha relations (Mitchner and Charles, 1973):

$$\frac{n_e n_1^+}{n_k} = 2\frac{g_l^+}{g_k} (\frac{2\pi m_e kT}{h^2})^{3/2} e^{-\varepsilon_{ik}/kT} \qquad (4)$$

where n_e is the free electron number density, n_1^+ is the number density of single ionized positive ions in the ground level and n_k is the number density of neutral particles in the k^{th} level.

Hydrodynamics. After the creation of the plasma, the expansion of the high-pressure plasma can be treated as the hydrodynamic motion. For simplification, only the one dimension hydrodynamic governing equation is shown (Vertes et al., 1989).

$$\frac{\partial \boldsymbol{R}}{\partial t} = -\frac{\partial \boldsymbol{F}}{\partial x} \quad (5)$$

where the components of the density vector, ***R*****,** are the mass density, momentum density and energy density

$R_1 = nm = \rho$, $R_2 = \rho v$,and

$$R_3 = \rho(e + v^2/2) \quad (6)$$

in terms of number density of the particles, n, mass of the particle, m, the hydrodynamic velocity, v, and the internal energy per unit mass, e. The generalized flux vector, ***F***, has the following components

$F_1 = \rho v$, $F_2 = p + \rho v^2$,and

$$F_3 = \rho v(e + P/\rho + v^2/2) - \Phi \quad (7)$$

where p denotes the pressure and Φ stands for the laser intensity. The laser intensity is determined by the laser absorption mentioned before.

$$\frac{d\Phi}{dx} = -k(x)\Phi \quad (8)$$

where $k(x)$ is the effective absorption coefficient.

Thermal energy transport and equation of state. Energy transported by the electrons and ions is modeled in the diffusion approximation for each fluid. The conservation equations of mass, momentum and energy can be closed by a constitute equation which relates the temperature *T*, density *ρ*, pressure *p*, energy *e* and other physical parameters of the material. The simplest equation of state is governed by the ideal gas law (Vertes, et al., 1989)

$$e = \frac{3}{2}(1+\eta)kT + \eta U \quad (9)$$

where *e* is the internal energy, k is the Boltzmann constant, η is the degree of ionization, and *U* is the ionization potential of the target material, *T* is the absolute temperature.

SIMULATION AND EXPERIMENT CONDITION

The coupled analysis of shock pressure generation and dynamic deformation process of the target material subjected to LSP was carried out based on the above principles. The simulation results were compared with that from two decoupled analysis schemes, in which, shock pressure generated either based on the above model or the model (Zhang and Yao, 2001) is used as loading in a subsequent FEM deformation analysis. The coupled analysis was implemented using a commercial radiation hydrodynamics simulation code, HYADES (CAS, 2001).

For the decoupled analysis, the deformation analysis was carried out using ABAQUS. Axisymmetric models with semi-infinite geometry were created for bulk targets similar to Zhang and Yao (2001), and 3D models with finite geometry were created for thin film samples similar to Zhang and Yao (2002b). A second type of comparison was also carried out, in which, HYADES generated shock pressure was used as loading in a subsequent FEM stress/strain analysis. In the FEM simulation, non-linear constitutive equations including work hardening, strain rate and pressure effects on yield strength of copper target are considered (Zhang and Yao, 2000).

Both bulk and thin film samples of copper were studied. Copper foils of 90-micron thickness were used as bulk samples. Thin film samples are prepared by physical vapor deposition (PVD) for 1-μm thick copper film and electrochemical plating (ECP) for 3-μm thick copper film on 0.5mm thick single crystal (004) silicon substrate. A 16-micron thick aluminum foil was used as the ablative coating layer for both bulk and thin film cases and foil was firmly attached to targets using vacuum grease. As seen from Fig. 1, a sample was placed in a shallow container filled with distilled water around 3 mm above the sample's top surface. A frequency tripled Q-switched Nd:YAG laser (wavelength 355nm) in TEM_{00} mode was used, the pulse duration was 50 ns, and pulse repetition rate could vary between 1 KHz to 20 KHz. Laser beam diameter is 12 microns and laser intensity was varied from 2 to 6 GW/cm^2.

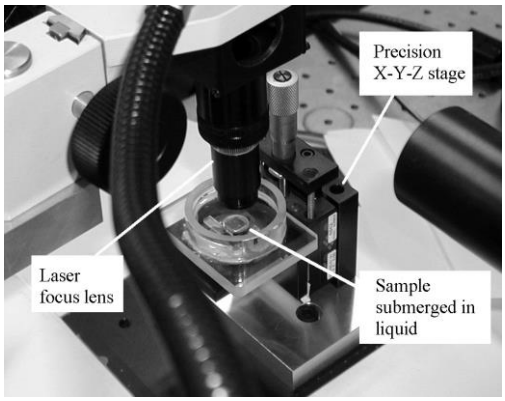

1. LSP EXPERIMENT SETUP

RESULTS AND DISCUSSION

Shock Pressure Comparison From Different Modeling Schemes

To facilitate discussions, the model (Zhang and Yao, 2001) used in the decoupled analysis is denoted as Model 1, while the coupled modeling as Model 2.

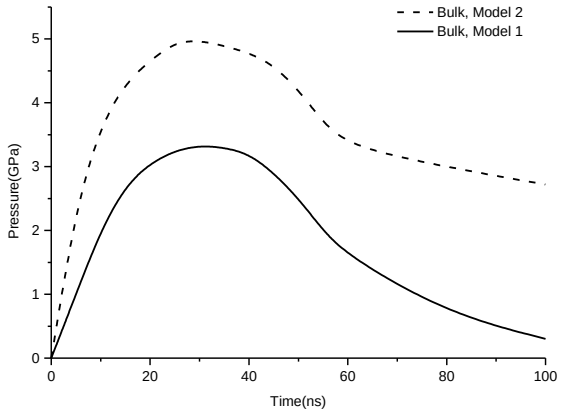

2. PRESSURE OF PLASMA IN LSP FROM DIFFERENT MODELS (COPPER BULK SAMPLE)

Fig. 2 compares the shock pressures between these two models under the same laser intensity ($I=4GW/cm^2$). As seen in Fig. 2, the shock pressure is higher and lasts longer as predicted by Model 2 than that by Model 1. Model 1 assumes that part of the laser energy is used for the breakdown of water and target besides the expansion of plasma. So the more mass flows from water and target into plasma due to breakdown, the less laser energy converts into the internal energy in the plasma. As a result, the pressure of plasma is lower and reduces to the atmosphere value faster. In Fig. 3, the density of different regions of water and Al coating layer are compared and it shows that the top layer of Al (zone 0, coating –water interface) is changed into the plasma as evidenced by the fast density decrease, while the region zone –1 (1μm below the coating surface) can be regarded as the molten layer and the zone –2 (2μm below the coating surface) is still in solid state. For the zone 0 of water (coating-water interface, 2μm thick in water) can still be regard as liquid which did not change into the plasma. Thus, the plasma generated in Model 2 is mainly from the breakdown of the Al coating layer and not from water. However, in Model 1, the mass flow from the water is one magnitude higher than from the metal target (Zhang and Yao, 2001) and the energy used to convert water to plasma was simply considered as the liquid to vapor phase change energy which is much lower than the energy needed for directly ionizing the water. So the water is more likely to convert into the plasma and much more laser energy is used to breakdown the water, thus, the shock pressure is lower in Model 1 than that in Model 2 and it decreases much faster as well.

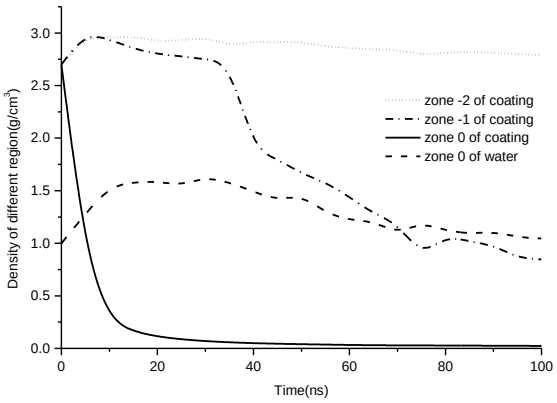

3. DENSITY AT DIFFERENT DEPTHS OF COATING LAYER AND CONFINED

Transient Processes and Deformation History In Target

Deformation History Analysis. Fig. 4 shows the transient deformation of the top surface of a bulk copper sample under LSP predicted by different modeling schemes. Result directly from Model 2 is compared with the top surface displacement from the result of FEM simulation with the shock pressure of Model 1 and 2. It shows that the deformation history from FEM simulation using Model 1 and 2 is in the same order and the value of Model 2 is slightly larger due to its higher shock pressure than that of Model 1 (Fig. 2). When comparing the FEM simulation result with that directly from Model 2, a major discrepancy is evident. As seen, during the initial stage of LSP (t<10ns, and pressure<2GPa), the deformation directly from Model 2 is consistent with the FEM simulation results. However, when time goes on, the deformation determined directly from Model 2 increases much more than FEM simulation results predicted and then rebounds. This can be explained by the different considerations about the

material response to shock wave adopted in these two models.

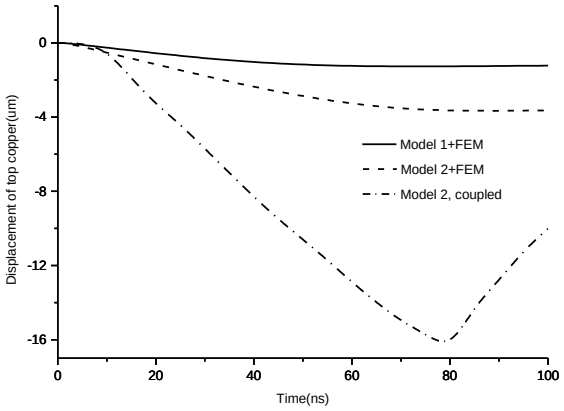

4. DISPLACEMENT HISTORY OF SURFACE OF BULK SAMPLES

In Model 2, the shock pressure is considered so high that strength effects can be neglected and the target can be treated as a compressible fluid which is known as the hydrodynamic approach. While in Model 1, shock pressure is used as a loading in FEM simulation which is based on the finite-plastic approach. Strength effect such as work hardening, strain rate and pressure effects on yield strength are considered in the FEM simulation (Zhang and Yao, 2001).

In the hydrodynamic approach, the equation of state is used to replace the non-linear constitutive equations in the FEM simulation. Also a shock Hugoniot curve can be obtained, in which one property versus others (such as P-V) behind the shock is depicted. When the shock pressure is low (i.e., t<10ns), the Hugoniot curve is very close to an isotropic path, which is usually the case for a solid under impact if the solid is only compressed slightly. Thus, the result from the hydrodynamic approach is consistent with the result from FEM simulation. When time goes on and pressure goes up, the target is compressed more such that both hydrodynamic and strength effect should be considered. The Hugoniot state (P-V) will be offset above the hydrostatic Hugoniot (which assumes hydrodynamic approach) due to strength effect (Fowles, 1960). Thus, in the hydrodynamic approach, a lower pressure is needed to achieve the same density. So for the same pressure, the material is easier to deform and the top surface displacement will be larger than the FEM simulation result.

Fig. 5 shows the deformation history for the 1μm and 3μm copper thin film predicted by the same simulation methods mentioned above. The deformation determined by the Model 2 based coupled method is again much larger than the decoupled results due to the same reason mentioned above. The deformation in the 3μm sample is slightly larger than the 1μm sample because a thicker film has a longer time to absorb the shock energy than a thinner film. Moreover, the slop of the deformation history which equals the particle velocity under shock (480m/s) is about twice as large as that of the bulk samples (Fig. 6). In thin film samples, the substrate is single crystal silicon as compared to copper in bulk samples. The impedance of single crystal silicon is about 1.97×10^7 kg/m^{2}s, smaller than that of copper (4.18×10^7 kg/m^{2}s). According to the wave-surface interaction analysis (Boslough and Asay, 1992), when shock wave propagates from the high-impedance material (copper thin film here) to the low-impedance material (silicon substrate here), the interaction will result in a reflected release wave back in copper and a transmitted shock in silicon which has a higher particle velocity due to its lower impedance. Thus, the shock wave can pass through the copper-silicon interface and propagate much easier and the hydrodynamic deformation will be larger than that in the bulk samples.

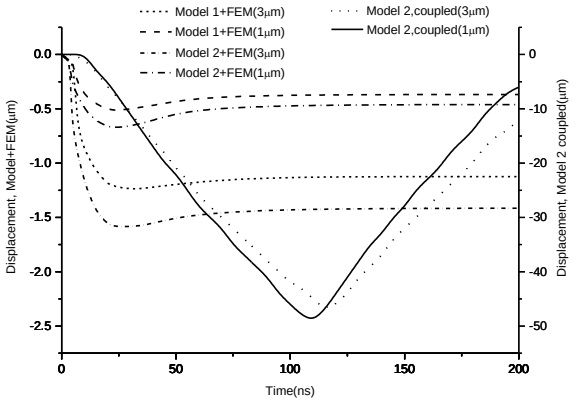

5. DISPLACEMENT HISTORY OF SURFACE OF THIN FILM SAMPLES

Laser Shock Wave Propagation. Consider a shock wave passing through the target, the states are undisturbed ahead of the shock front and the target is compressed behind the shock, so shock front position and shock velocity can be determined if deformation history in the depth direction is known. In Fig. 6, from the Model 2

based coupled analysis, the particle velocity, that is, the slop of the deformation history curve, is about 240m/s, and the shock velocity, that is, the slop of the straight line which connects the shock front at different times, is about 2km/s. From the decoupled results, the particle velocity is 120-160m/s, while the shock velocity is about 4.14km/s. The discrepancy is explained as follows.

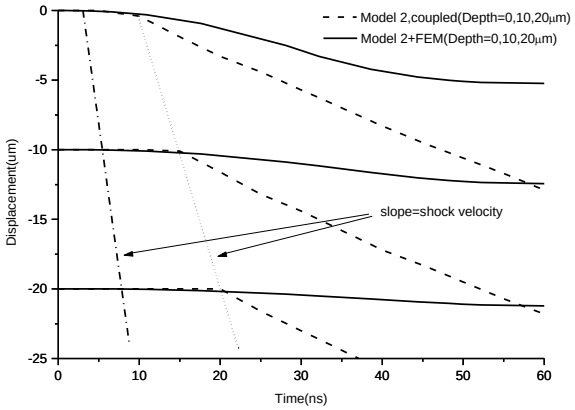

6. DISPLACEMENT HISTORY IN DIFFERENT DEPTHS OF BULK COPPER TARGET (0, 10 and 20 μm BELOW THE TOP SURFACE, LASER INTENSITY I=4GW/cm^2)

Examining the material response parameters under shock impact, the shock velocity of copper is $U=C_0+Su$, where C_0 (3.94km/s) is the sound velocity in copper, S=1.489 (Assay and Shahinpoor, 1992) and particle velocity u=135m/s under 5GPa shock pressure as determined above. This gives U=4.17km/s, which is very close to that determined by the decoupled analysis shown in Fig. 6. This is because in the FEM portion of the decoupled analysis, non-linear constitutive equations including work hardening, strain rate and pressure effects on yield strength of the copper target are considered and they are comparable with the Hugoniot data obtained from material experiments. In the Model 2 based coupled analysis, the shock velocity (2km/s) is close to that of water, which is around 2.1km/s for the same particle velocity. This is because that under the hydrodynamic approach employed by the coupled analysis, the target material is considered as a compressible fluid.

As seen from Figs. 4 and 5, the deformation curves determined by the Model 2 based coupled analysis reverse their direction at a certain time. When a shock front propagates to reach the bottom surface of the target, the rarefaction wave (release wave) is reflected back and cancels part of the original incoming shock wave so that the total pressure decreases. In the hydrodynamic approach employed by the Model 2 based coupled analysis, the target material will expand when the pressure decreases by behaving like a compressible fluid or gas. Thus, the deformation reverses its direction at that time.

STRAIN MEASUREMENT VIA X-RAY MICRO-DIFFRACTION

Measurement Principle

LSP induced strains were measured to compare with that predicted by simulation. In the diffraction intensity contrast method (Noyan et al., 1998), the X-ray micro beam penetrates the thin film to reach the silicon substrate and the diffraction intensity of the single crystal substrate is recorded. The stress/strain in the substrate was coupled to by the LSP deformed thin film. The increase of diffraction intensity comes from the increased mosaic structure in the substrate under the influence by the stress/strain field in the thin film at the interface (Noyan et al., 1998). An index to evaluate this combined effect is strain energy density D defined as (Ventse and Krauthammer, 2001)

$$D = \frac{1}{2}\varepsilon_{ij}\sigma_{ij} = \frac{1}{2}(\varepsilon_{11}\sigma_{11} + \varepsilon_{22}\sigma_{22} + \varepsilon_{33}\sigma_{33} + \varepsilon_{12}\sigma_{12} + \varepsilon_{13}\sigma_{13} + \varepsilon_{23}\sigma_{23}) \quad (10)$$

where ε_{ij} is the total strain tensor and σ_{ij} the residual stress tensor at the thin film/substrate interface. The unit of D is J/m^3.

Measurement Results and Comparison With FEM Simulation

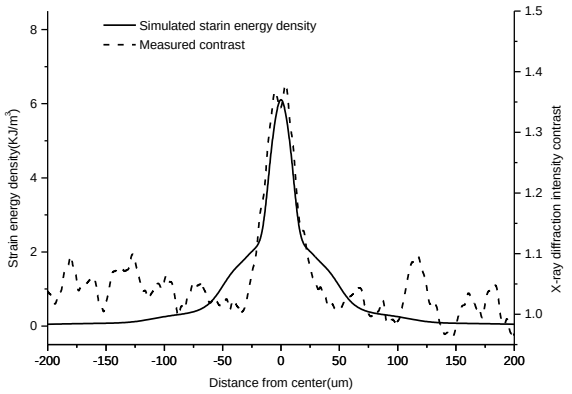

(a)

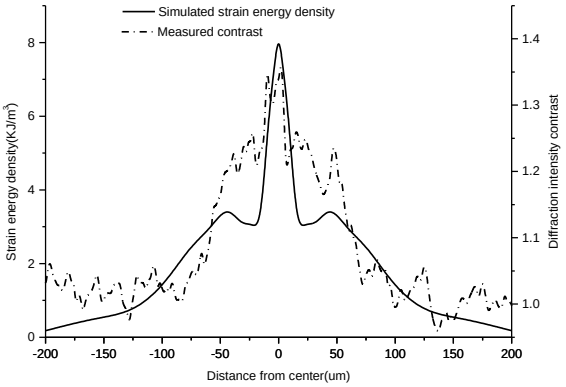

(b)

7. COMPARISION OF SIMULATED STRAIN ENERGY DENSITY AND X-RAY INTENSITY CONTRAST MEASUREMENT (LASER ENERGY I=280μJ)

Fig. 7 correlates the diffraction intensity contrast curves with the FEM determined stain energy density (Eq. 10). (a) shows that they match very well for the single-line shock case and (b) shows they exhibit a similar pattern for the three-line shock case. The agreement is expected; but to further understand the correlation, it is important and interesting to explore the strain coupling status at the thin film and substrate interface.

Fig. 8 illustrates the variation of individual strain components in (a) the 1μm thin film copper and (b) the silicon substrate at their interface determined by the FEM simulation. In copper, the normal strain *E11*, *E22*, and *E33* are dominant as compared with the shear stresses. In-plane strain *E11* and *E22* are both compressive and have a similar magnitude to each other, which indicates an equi-biaxial plane strain distribution. The depth-direction strain, *E33*, is tensile according to the volume conservation through Poisson's ratio and consistent with the maximum principal elastic strain. Across the interface, a corresponding strain field balancing the residual stress in the copper layer exists in the silicon layer. In (b), the normal strains in silicon are smaller compared with the shear strains. As mentioned before, the shear stress or shear strain in silicon is due to the non-uniformity of stress/strain in the copper layer at the interface. Silicon has a higher Young's modulus than copper so that the strain values in the silicon are smaller than that in the copper under the same level of stress.

From the analysis above, it is clear that elastic strain concentration exists in the silicon substrate through the strain coupling across the interface and it causes the silicon deform in the shock-affected region and this deformation will changes the initially perfect single crystal to an imperfect single crystal so that X-ray diffraction intensity increases in this shock-affected region.

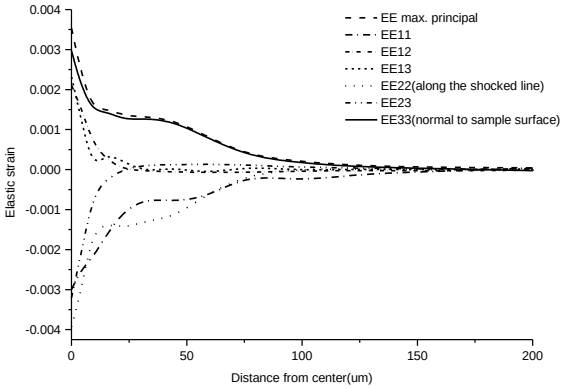

(a)

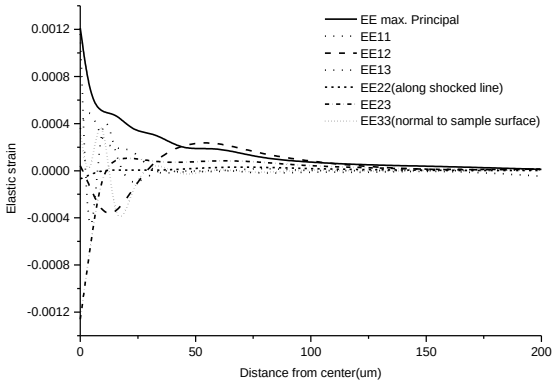

(b)

8. STRAIN COUPLING AT THE COPPER-SILICON INTERFACE, SHOCKED AT 350μJ.

CONCLUSIONS

Three modeling schemes were considered: (1) coupled analysis based on Model 2, (2) decoupled analysis based on Model 1 and FEM, and (3) decoupled analysis based on Model 2-determined shock pressure as loading in FEM. Strain measurements based on the diffraction intensity contrast method agreed with the strain energy density determined by the modeling scheme 3, indicating it may represent a good compromise in capturing the physics of micro-scale LSP. Shock pressure obtained from scheme 1 has a higher amplitude and lasts longer as compared with that from scheme 2. This is likely to be correct because scheme 2

assumed part of laser energy was used to breakdown water while this is true only when the laser intensity is very high. An advantage of scheme 1 is many transient quantities such as particle velocity can be directly obtained. Results show the dynamic deformation is much larger if obtained under scheme 1, which assumed the target deformation under shock is hydrodynamic, than that under other two schemes, in which the FEM simulation considered the target response as a finite-plastic process and material strength effect was included. This is likely to be incorrect because the particle and shock velocity of the target material (copper) determined through the FEM in schemes 2 and 3 are consistent with the tabulated Hugoniot data.

ACKNOWLEDGMENT

This work is partially supported by the National Science Foundation under grant DMI-02-00334. Support by Columbia University is gratefully acknowledged. Valuable discussions with Dr. W. Zhang of GE Global Research Center are also greatly appreciated. HYADES code was made available through Cascade Applied Sciences, Inc. Dr. I. Cev Noyan of IBM Watson Research Center provided guidance and permission to access X-ray microdiffraction apparatus at the National Synchrotron Light Source at Brookhaven National Laboratory.

REFERENCES

Assay, J. R., and Shahinpoor, M., (1992), *High-pressure Shock Compression of Solids*, New York, Springer-Verlag, pp. 379.

CAS (Cascade Applied Sicences, Inc.), (2001), *HYADES Professional and HYADES Professional Plus*.

Clauer, A. H., and Holbrook, J. H., (1981), "Effects of Laser Induced Shock Waves on Metals," *Shock Waves and High Strain Phenomena in Metals-Concepts and Applications*, New York, Plenum, pp. 675-702.

Fabbro, R., Fournier, J., Ballard, P., Devaux, D., and Virmont, J., (1990), "Physical Study of Laser-produced Plasma in Confined Geometry," *J. Appl. Phys.*, Vol. 68(2), pp. 775-784.

Fowles, G.R., (1960), "Attenuation of the Shock Wave Produced in a Solid by a Flying Plate, *J. Appl. Phys.*, Vol. 31, pp. 655-661.

Mitchner, M., and Charles H.Kruger, (1973), "Collisional and Radiative Process", *Partially Ionized Gases*, New York, John Wiley &Sons, pp75-79.

Noyan, I. C., Jordan-sweet J. L., Liniger, E. G., Kaldor, S. K., (1998), "Characcterization of Substrate/Thin-film Interfaces with X-ray Microdiffraction," *Applied Physics Letters*, Vol., 72(25), pp. 3338-3340.

Root, Robert G. (1989), "Modeling of Post-Breakdown Phonomena", *Laser-induced Plasmas and Applicaions*, New York, Marcel Dekker, pp 72-75.

Ventsel, E. and Krauthammer, T., (2001), *Thin Plates and Shells: Theory, Analysis and Applications* , New York, Marcel Dekker, Inc., pp. 37.

Vertes, A., Juhasz, P., Dewolf, M., and Gijbels, R., (1989), "Hydrodynamic Modeling of Laser Plasma Ionization Processes", *International Journal of Mass Spectrometry and Ion Processes*, pp. 63-85.

Weyl, Guy M. (1989), "Physics of Laser-Induced Breakdown: An Update", *Laser-induced Plasmas and Applicaions*, New York, Marcel Dekker, pp 48-49.

Zhang, W. and Yao, Y. L., (2000), "Improvement of Laser Induced Residual Stress Distributions via Shock Waves," *Proc. ICALEO'00, Laser Materials Processing*, Vol. 89, pp. E183-192.

Zhang, W. and Yao, Y. L., (2001), "Modeling and Simulation Improvement in Laser Shock Processing," *Proc. ICALEO'01,* Section A.

Zhang, W. and Yao, Y. L., (2002a), "Micro Scale Laser Shock Processing of Metallic Components," *ASME Journal of Manufacturing Science and Engineering*, Vol. 124, No. 2, pp. 369-378.

Zhang, W. and Yao, Y. L., (2002b), "Micro Scale Laser Shock Penning of Thin Films", *ASME Journal of Manufacturing Science and Engineering*, under review.